THE VORTEX IMPULSE THEORY FOR FINITE WINGS

Shiang Yu Lee

Chief Scientist, LW Aero science, 583 Battery Street Unit 2106N,
Seattle WA

ABSTRACT

Based on the observation that lift producing circulation is the result of divergent reflective flows circumventing planform edges, this research presents a comprehensive new theory for finite rectangular wing aerodynamics. First the study presents a new expression for potential lift, emphasizing geometrical effects that reduce circulation strengths and lifting capacity. Second, a novel "crossflow separation vortex normal force" is derived through the application of the long-overlooked Milne-Thompson "Vortex Impulse Theory." The vortex force turns out surprisingly to be a linear function of the angle of attack. An empirical non-linear pressure drag normal force relationship is also provided to complement the linear theories. Since crucial experimental evidence shows that potential lift is absent in narrow wing cases, it is excluded in that *range and only provides restricted contributions in wider configurations. This unique three element lift theory is proven to provide consistent and accurate predictions for all geometry ranges.*

KEYWORDS

Aerodynamics, Airplane, Wing, Vortex, Circulation, Navier Stokes Equations, Lift

1. INTRODUCTION

It is widely acknowledged that finite rectangular wings, or flat plates, experience significant lift degradation as the aspect ratio decreases. This has been demonstrated in the classical Prandtl-Betz [1] experiments, Fig. 1, where it was found that a square wing only has a quarter of the lifting capacity compared to very wide wings. On the other hand, stable flow can be sustained to very high angles of attack for narrow wings in the presence of wingtip vortex separation, enabling very high lift. Classical theories, such as the Prandtl Lifting Line Theory (LLT) [2] and ensuing developments along the same approach, do not appear to recognize the likelihood of lift generation by the trailing vorticities. In fact they focus on the vortices' roles in causing the downwash flow which reduces the effective angle of attack and, consequently, the circulation and lift strengths as well as producing the lift-induced drag. Neither did the Trefftz plan analysis, which should be the most appropriate approach, appear to succeed in identifying and establishing the crossflow vortex contributions.

DOI : 10.5121/mathsj.2025.12201

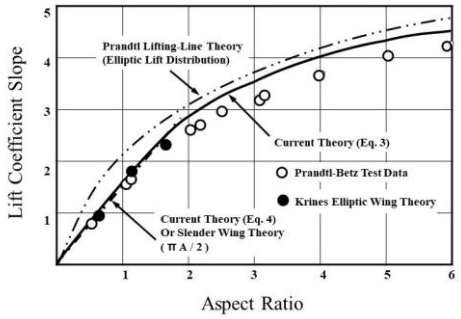

Figure 1 Lift Coefficient Slope as Function of Aspect Ratio

There were several early attempts in non-linear aerodynamic force analyses, but none seem to evolve into a well-established theory. Detailed review of existing theories can be found in many books in the field, such as Schlichting, et. al. [3] for linear theories and Rom [4] for non-linear model developments. Hoerner [5] evaluated experimental data against the linear lift described by the Slender Wing Theory (SWT, see, for example in [3]), and observed that there are substantial lift discrepancies which must be compensated by an additional lift element. He identified the difference as a "second lift" and ascribed it to a non-linear term requiring very high lift coefficient slope values. The Leading-Edge Suction Analogy (LESA) [6], proposed by Polhamus for delta wings and extended by Lamar [7] to rectangular wings and other planforms, applied a vortex force of significant magnitude in the solutions. These solutions provided apparent accurate predictions, establishing their prevalence in the field.

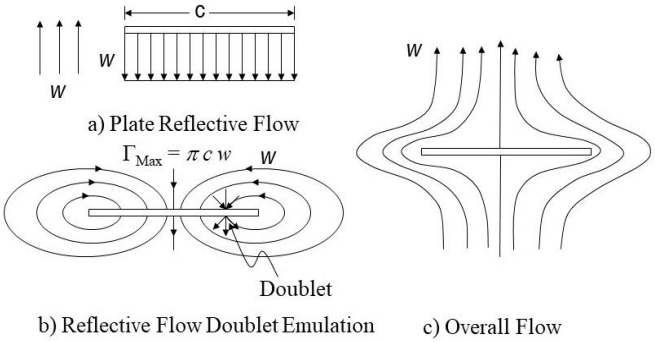

Figure 2 Reflective Flow on a Narrow Moving Plate

This study attempts a non-traditional approach and provides a new theory for finite rectangular wing aerodynamics. Based on the assumption that lift producing circulation is the consequence of divergent reflective flows of the incoming stream, circumventing the planform edges, a direct determination of the bound circulation and separation vortex configuration is attempted, together with identifying their distinct force contributions. Accordingly, a set of alternative potential lift coefficient expressions is developed and, since the spreading flow also fosters crossflow wingtip separations, a separation vortex normal force is derived. This is accomplished through the application of a long-overlooked "vortex impulse theory" originally introduced by Milne-Thomson [8]. This approach was first attempted by Lee [9] but refined and extended here. In addition, an empirical approximation for the non-linear normal force is provided based on experimental data. Furthermore, critical evidence reveals that potential lift is, in fact, absent in low aspect ratio cases; it is therefore excluded in this range and adjusted for wider planforms.

This novel three-force aerodynamic theory is validated by the highly accurate predictions against all experimental data.

2. THEORY DEVELOPMENT

2.1. Reflective Flow Geometry

According to the potential flow theory, a submerged, two-dimensional flat plate moving at constant velocity normal to its surface, the resulting reflective flow can be modeled by a set of distributed doublets along its width, Fig. 2 a. Nonetheless, Katz [10] stated that this doublet configuration is equivalent to two vortices located at the ends of the plate. This led to the assumption of a reflective flow pattern with circular trajectories and constant tangential velocity streaming around the plate edges, as depicted in Fig. 2 b. This flow pattern could be considered as a "forced flow" field, it features a linear circulation distribution with the maximum circulation (strength of πcw, determined through integration over the circular trajectory) located at the centre line.

Understandably, this flow pattern cannot persist, separations must occur, and one can hardly ever observe the initial reflective flow as described. Nevertheless, the separation vortices along the edges of an inclined narrow rectangular wing are, in fact, a perfect manifestation of the separation process: the vortices rising up along the edges record the history of separation transients, establishing a steady pattern.

Returning to the case of Fig. 2, if the plate also moves sideways, the downstream vortices will have to slip off into the wake to form the starting vortex whereas the forward flowing front vortices will wrap around the wing to form the bound circulation. This circulation will adopt the maximum value, $\Gamma_{Max} = \pi c w = \pi c V \sin\alpha$, yielding the Kutta-Joukowsky flat plate solution configuration.

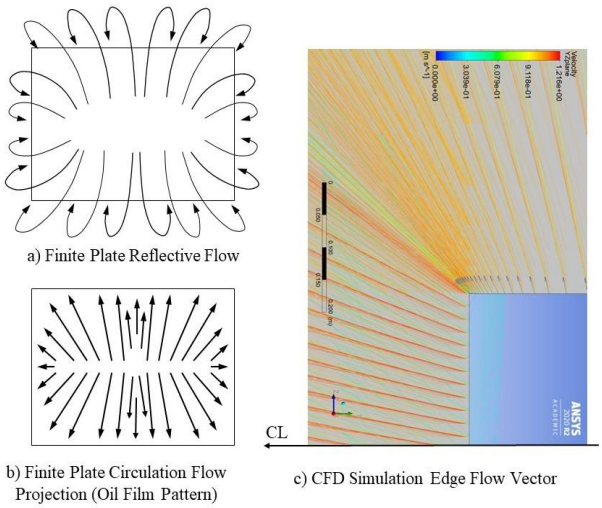

Figure 3 Finite Plate Reflective Flow

Now, for the case of a finite wing, the reflective flow on the impact side must spread out divergently before circling to the back side of the plate, Fig. 3. Particularly, for a circular or square planform, assuming a finite wind-tunnel-like passage, in order to maintain continuity, the

recirculating flow passage must be confined to a racetrack area with reduced depth as shown by the grey areas in Fig. 4. By observation, in order to maintain continuity, the dimension of the outer passage must be √2 times the inner plate. This configuration entails a maximum circulation strength $\Gamma_{Max} = \frac{w\pi d}{\sqrt{2}}$, a significant reduction from the long plate case. This maximum circulation value is assumed to prevail around the entire planform.

When the planform geometry flattens out to higher aspect ratios, again, by assuming constant outer passage width and equal areas, it provides that approximately, a relation $d' \cong \frac{2Ad}{\sqrt{1+A^2}}$. This relationship has been verified numerically to be effective for all aspect ratios. Consequently, the maximum circulation then becomes:

$$\Gamma_{Max} = \frac{Aw\pi d}{\sqrt{1+A^2}}. \tag{1}$$

This result implies that when the aspect ratio is reduced, so does the maximum circulation and lifting capacity. When the tunnel wall restriction is removed leaving an open domain, it is assumed that the maximum circulation values will endure and remain unchanged.

2.2. The Potential Lift

A potential lift, in the context of this paper, is defined as a lifting force resulting from the bound circulation on the wing interacting with the free stream flow, or simply, the Kutta-Joukowsky lift. It is identified here to distinguish it from lift generated through other mechanisms to be developed.

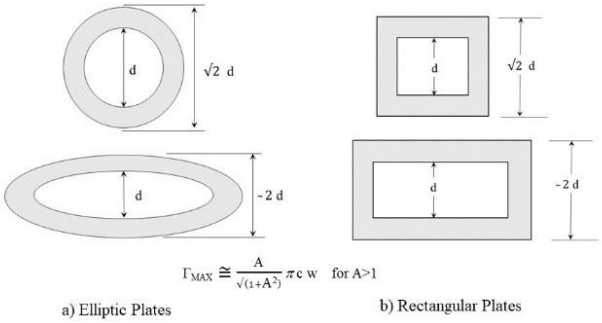

Fig. 4 Finite Plate Reflective Flow in Closed Passages

According to classical potential flow theory, in the case of thin wings or flat plates, this force is accompanied by a leading-edge suction force so that the resultant force is normal to the free stream flow instead of the wing surface. Conversely, a resultant force normal to the wing planform rules out the potential lift or leading-edge suction.

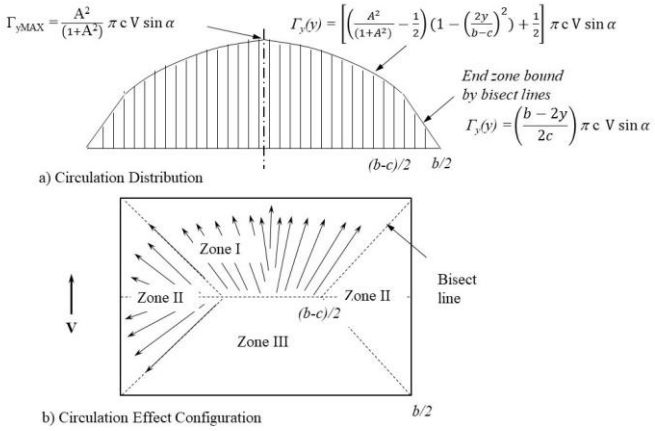

Figure 5 Finite Plate Circulation Evaluation

For finite wings, as seen in the CFD simulation in Fig. 3 c, the reflective flow at the centre of the plate is slanted toward the edges. It is assumed that the reflective circulating flows, flowing in flat vertical planes that follow a divergent pattern, will leave straight traces on the plate surface, in patterns resembling a palm tree leaf or bird feather barbs.

According to the observation made in this study, the reflective flow could be divided into four regions as shown in Fig. 5 b. Zone I, located at the forward part of the plate, is where the circulation wraps around the leading edge to form the lift-producing circulation. Zone II, on both sides of the plate, bounded by the bisect lines, is where crossflow separation vortices form and then propagate downstream as wingtip trailing vortices. For Zone III, located on the trailing edge side, the circulations drift into the wake to form the "starting vortex". Once the starting vortex shedding occurs, like the two-dimensional case discussed earlier, the flow on the wing quickly evolves into a steady state. The appropriate boundary conditions will be satisfied automatically, resulting in the lift producing circulation configuration.

The hypothesis put forth in this study asserts that the fully developed wing circulation is dependent on the initial reflective flow orientation and distribution at the onset of motion. The local potential lift, which is defined as the lifting force resulting from the interaction between the bound circulation and the free stream flow, or as the inner product of the circulation and the free stream flow. Furthermore, it is assumed that the lift is determined at the circulation starting points along the mid-chord centreline to realize the maximum circulation and lift. This remains true until reaching the intersection of the bisect lines near the wing tip, (b-c)/2. Beyond this point, no circulation originating from the centreline can reach the leading edge, and therefore, cannot contribute to the potential lift.

For this edge section, the potential lift is provided by the component projection of the circulation flowing along the bisect lines. This portion of lift decreases linearly to zero at the tip corner of the plate as the circulation is dependent upon the distance from the apex, as shown in Fig. 5 a. This is especially true for the square plate and narrower cases where the effective lifting circulations are only those projected components from the circulations along the bisect lines.

Proceeding now to the determination of potential lift, at the centre span (y=0), the slanting of the circulation is assumed to conform to the rectangle geometry. This means the projection components are inversely proportional to the distances from the nearby edges, as suggested by

the CFD results in Fig. 3, that is, $\frac{\Gamma_y(0)}{\Gamma_{Max}} = \frac{A}{\sqrt{1+A^2}}$. Accordingly, this results in the highest projected y component of lift producing circulation, at the centre of the plate, to be,

$$\Gamma_{yMAX}(0) = \frac{A^2}{(1+A^2)} \pi c V \sin\alpha \tag{2}$$

Since this circulation component assumes a maximum value at the centreline but gradually reduces to the reduced value of $\pi c V \sin\alpha /2$ at the intersection of the bisect lines, y= (b-c)/2, the distribution can be approximated by a parabolic curve, Fig. 5 a. Beyond this point, the circulation is the projection from the bisect line, and its distribution varies linearly as mentioned earlier. Thus, the total lift can be evaluated through classical potential lift definition, for A>1, as,

$$C_{LP} = 4/(\rho bcV^2)\int_0^{b/2}(\rho \boldsymbol{V}\cdot\boldsymbol{\Gamma})dy = 4/(bcV^2)\int_0^{b/2}(V\Gamma_y)dy$$

$$= \left(\frac{4\pi c \sin\alpha}{b}\right)\left\{\int_0^{\frac{b-c}{2}}\left[\left(\frac{A^2}{(1+A^2)}-\frac{1}{2}\right)\left(1-\left(\frac{2y}{b-c}\right)^2\right)+\frac{1}{2}\right]dy + \int_{\frac{b-c}{2}}^{\frac{b}{2}}\left(\frac{b-2y}{2b}\right)dy\right\}$$

$$= 2\pi \sin\alpha \frac{\left[\left(\frac{2A^2}{3(1+A^2)}+\frac{1}{6}\right)(A-1)+\frac{1}{4}\right]}{A}$$

$$= 2\pi \sin\alpha \left[\left(\frac{1+5A^2}{6(1+A^2)}\right)(A-1)+1/4\right]/A$$

$$= C_{LP\alpha}\sin\alpha \tag{3}$$

In the above derivation, for simplicity, the effect from free stream flow induction is omitted. It can, however, be easily incorporated if the situation warrants.

It is seen that for A<1 (narrow wing cases), potential lift is limited to the triangle area bound by the bisect lines at the front tip area. The lift coefficient, after proper adjustments to the circulation expression, becomes:

$$C_{LP} = \frac{2}{bcV^2}\int_0^{\frac{b}{2}} VA\Gamma c/2\left(\frac{b-2y}{2b}\right)dy = \frac{1}{bcV^2}\int_0^{\frac{b}{2}} V(\pi Ac)\,V\sin\alpha\left(\frac{b-2y}{2b}\right)dy$$

$$= A\pi \sin\alpha /2 = C_{LP\alpha}\sin\alpha \tag{4}$$

The values of Eq. 3 and Eq. 4 are added to Fig. 1 for comparison with experimental results. It is seen that for narrow wings, Eq. (4), the lift distribution, although derived through a different logic, is consistent with the SWT prediction. For higher aspect ratios, the values are slightly higher than the experimental data. The overall accuracy and applicability of the potential lift will be addressed later in this paper.

2.3. Vortex Normal Force

The vortex normal force is the force exerted on the wing as it spawns crossflow trailing vortices. The Milne-Thomson vortex impulse theory states that, if there is a circular ring vortex with strength Γ and area S, the flow system could be considered as the result of an impulse, I (Fig. 6), applied to the ring area. If the area continues to grow, the force causing the growth of the vortex ring can be computed through Newton's law of impulse-momentum change, as:

$$\boldsymbol{F} = \frac{d}{dt}(\boldsymbol{I}) = \frac{d}{dt}(\rho\Gamma\boldsymbol{n}S) = \rho\Gamma\boldsymbol{n}\frac{d}{dt}(S) \quad (5)$$

where **n** is a unit vector aligned with the impulse force.

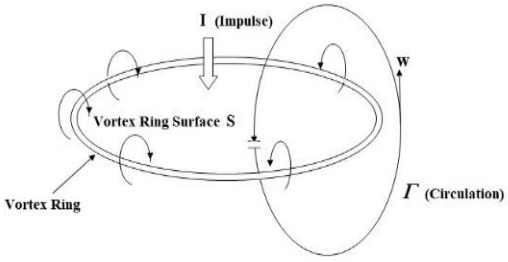

Figure 6 Vortex Ring Impulse

For a rectangular wing in motion, the growing vortex ring is then simply the area bound by the starting vortex, the trailing vortices, and the wing itself. According to Milne-Thomson, the growing ring area, for any span increment, is simply dS=Vtdy, a linear function of time. This expression can be used in Eq. 5 to evaluate the forces applied.

Proceeding now with investigating the vortical flow, denoted as Γ_x, around side edges for A>1 (Fig. 7). This vortex system, like the forward wrapping circulation, is also confined by the bisect lines and does not extend inward beyond their intersection at (b-c)/2. For narrow wings, A<1, the separated vortical flows cover the entire span but they are also affected by the slanting effect. Evidently the circulations have the highest strength at the centre line of the chord (Fig. 8a). The crossflow vortex component, Γ_x (noticing that the vortices are circling around the side edges), has a maximum value analogous to Eq. (4): $\Gamma_{xMAX} = \frac{1}{(1+A^2)}\pi b V \sin\alpha$.

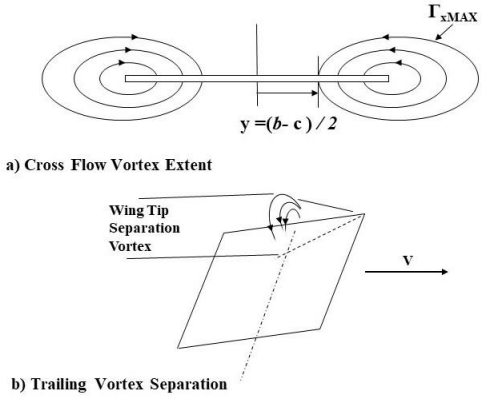

Figure 7 Finite Plate Reflective Crossflow Circulation Distribution

It is helpful to imagine that the "vortex ring" of the trailing vortices, formed by the reflective flow circulations extending into the wake, Fig. 7 a), appears to be frozen. This conceptual freezing enables the determination of the vortex distribution along the span, even though these vortices will quickly evolve into a separated spiralling vortex. By observation, the strongest vortices drifting into the wake are initiated at the centre line. For narrow wing cases (A <1), the circulation flow, resembling a palm branch pattern, extends from the centre to the edge along the mid-chord, with progressive inclination toward the edge (Fig. 8 a).

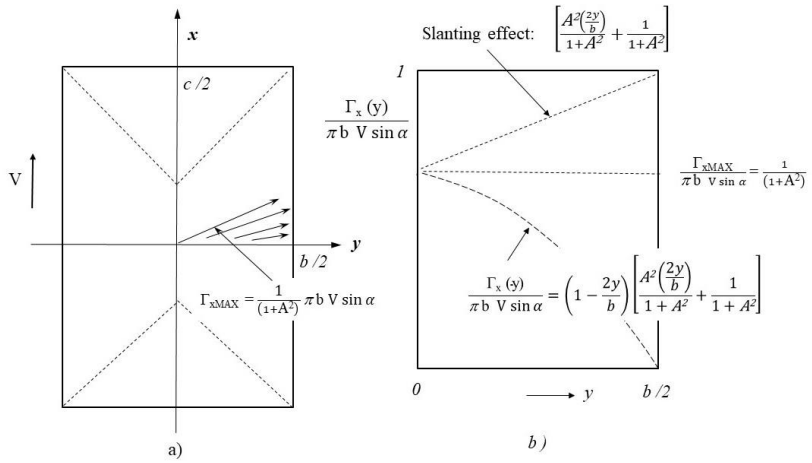

Figure 8 Narrow Wing Mid-Chord Cross Flow Separation Vortex Evaluation

As an approximation, it is assumed that this progressive slanting effect follows a simple linear distribution, see Fig. 8 b. Thereby the vortex distribution, including the edge distance effect, becomes:

$$\Gamma_x(y) = V\pi b \sin\alpha \left(1 - \frac{2y}{b}\right) \left[\frac{A^2\left(\frac{2y}{b}\right)+1}{1+A^2}\right] \tag{6}$$

Consequently, the force of the separation vortex, can be evaluated as:

$$C_{NV} = \left[\frac{2}{\rho bcV^2}\right]\frac{d}{dt}\left(\int_{(s)} \rho\Gamma_x dS\right) = \left[\frac{2}{bcV^2}\right]\frac{d}{dt}\left(\int_{(s)} \Gamma_x V t dy\right)$$

$$= \left[\frac{2}{bcV^2}\right]\int_0^{\frac{b}{2}} \Gamma_x(y) V dy = \left[\frac{4}{bcV^2}\right]\int_0^{\frac{b}{2}} V\pi b \sin\alpha \left(1 - \frac{2y}{b}\right)\left[\frac{A^2\left(\frac{2y}{b}\right)+1}{1+A^2}\right] V dy$$

$$= 2\pi A\left[\frac{3+A^2}{6(1+A^2)}\right] \sin\alpha = C_{NV\alpha} \sin\alpha \tag{7}$$

Note that the force is imparted by the wing to the air passing by, forcing it into vortices normal to the wing surface; it is therefore identified as the "crossflow separation vortex normal force". Significantly, this is a linear function of sinα.

Since the side edge separation vortices do not exceed the bisect line boundaries, the vortex force coefficient slope, $C_{NV\alpha}$ reaches a maximum value of 2.09 at A=1. On wider wings (A>1), this maximum vortex force (achieved at A=1) is assumed to be distributed over a larger relative area, or its influence is concentrated at the tip. Therefore, the overall normal force coefficient for the entire wing becomes:

$$C_{NV} = 2.09 \sin\alpha/A = C_{NV\alpha} \sin\alpha \tag{8}$$

This $C_{NV\alpha}$ of approximately 2.09 at A=1, is the same value as the potential lift coefficient slope of the Prandtl elliptic wing LLT theory. The difference is that here the value stands for the force caused by the reflective separation vortex and therefore is normal to the plate. In evaluating the overall aerodynamic forces, the lift component of this normal force (i.e. projected onto the direction perpendicular to the freestream) is lower than the LLT potential lift value by a factor of cosα, enabling better agreement with experiments. On the other hand, the streamwise projection

of this force provides a substantial contribution to the drag, as an alternative to the "lift-induced drag".

For wide wings, these vortex forces are concentrated near the wing tip area. Careful measurement of wing root up-bending moments could verify the unique predictions of this theory. This element could also play a significant role in the directional stability of airplane flight dynamics. Reference [9] was a first attempt by this author to apply the vortex impulse theory to a finite rectangular wing. That effort fell short of discovering all relevant force elements and committed some mathematical errors. The current work is an effort to complete the research.

2.4. The Pressure Drag

The notion of "pressure drag", as described by Hoerner in [11], is the force exerted on a solid body due to flow separation causing a turbulent wake. Here, it is assumed that a wing inclined in the flow field also could incur normal forces. These forces are caused by the projected normal flow component and, particularly when stalling occurs partially or fully. These effects are amply documented in experiments. The force is recognized as the non-linear normal force component, consistent with Newton's theory (which provides both lift and drag to the wing), and is commonly referred to as the "sine square law". However, except for wings in supersonic flows, this force does not appear to have been properly treated in the literature.

For very high subcritical Reynolds numbers and high aspect ratio, the fully stalled drag coefficient assumes the value of 2, as given by Newton and confirmed by experiments. On the other hand, for an aspect ratio of unity (a square plate), the value reduces to a minimum of 1.17, according to Winter's experiments [12]. Apparently, the drag force is, again, governed by the planform geometry.

An empirical formula is then established, for this study, to represent the variations by adopting a simple "area rule" representation. That is, for A<1, since the side edge separation vortices are always present:

$$C_{NN} = [1.17A + 2(1 - A)]\, sin^2\, \alpha \; = C_{NN\alpha}\, sin^2\, \alpha \tag{9}$$

This is based on the recognition that once the side edge separation occurs, the entire wing is in a stalled state and the pressure drag will be fully present, complementing the vortex normal force. Similar to the potential lift, the front and back end zone areas are also assumed to produce lowered pressure drag, while the remaining areas suffer full drag effects.

On the other hand, consider wider wings (A>1) before leading-edge separation stalling occurs. In this regime, potential lift is effective, and only the side edge regions with crossflow separation are assumed to cause a pressure drag. Therefore:

$$C_{NN} = 1.17\, sin^2\, \alpha\, /A = C_{NN\alpha}\, sin^2\, \alpha \tag{10}$$

Similar to the vortex normal force, this pressure drag force is also expected to also be exerted primarily on the wing tip areas.

Finally, after leading edge stalling occurs, the entire wing is immersed in the turbulent wake. This suggests a force expression like the narrow wing case (Eq. 9):

$$C_{NN} = [\tfrac{1.17}{A} + 2\left(1 - \tfrac{1}{A}\right)]\, sin^2\, \alpha = C_{NN\alpha}\, sin^2\, \alpha \tag{11}$$

In this post-stall condition, the force is distributed over the entire span.

2.5. Applicability Conditions

Before applying the above results, it is prudent to reexamine experimental evidence in detail to determine the proper representation of the physical facts. Fig. 9 shows the drag-over-lift ratio from the Lamar data [7]. It is seen that, for cases of low aspect ratio, all the data fall right on the tan α line. Any data point below the tangent curve would indicate the presence of leading-edge suction or potential lift, but that, apparently, is not the case here. This is to say that, for low aspect ratio wings, there really is no "potential lift" present, only normal forces!

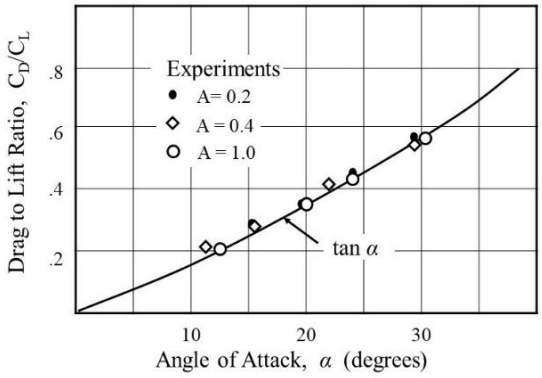

Figure 9 Drag to Lift Ratio for A<1

It can be reasoned that for A<1, since the side-edge separation vortex disturbances extend all the way to the centreline, so that the entire span of the wing is stalled, disturbing the Kutta condition, and there really could not be any bound circulation or potential lift present. Following the same logic then, for a wider wing (A>1, Fig. 7), the wingtip area bound by the bisect lines is in the flow separation stalled state and, consequently, Eq. (4) could be truncated to the bisect line intersections, as,

$$C_{LP} = \left(\frac{4\pi\, cV \sin\alpha}{b}\right)\{\int_0^{\frac{b-c}{2}} \left[\left(\frac{A^2}{(1+A^2)} - \frac{1}{2}\right)\left(1 - \left(\frac{2y}{b-c}\right)^2\right) + \frac{1}{2}\right] y dy\}$$
$$= 2\pi \sin\alpha \left[\left(\frac{1+5A^2}{6(1+A^2)}\right)(A-1)\right]/A = C_{LP\alpha} \sin\alpha \qquad (12)$$

So that potential lift is available only in the mid-span region.
With these understandings, the overall lift force expression is therefore,

$$C_L = C_{LP\alpha} \sin\alpha + C_{NV\alpha} \sin\alpha \cos\alpha + C_{NN\alpha} \sin^2\alpha \cos\alpha \qquad (13)$$

These terms are identified as the potential lift, the linear crossflow vortex normal force lift and the non-linear pressure drag lift, respectively. Whereas the total drag is evaluated as,

$$C_D = C_{NV\alpha} \sin^2\alpha + C_{NN\alpha} \sin^3\alpha \qquad (14)$$

Summarizing the above discussions, Table 1 lists the applicability of each aerodynamic force element with respect to the aspect ratio ranges, as well as the stalling conditions.

Table 1 Applicability Conditions of Aerodynamic Coefficients

	A <1	A > 1 Pre-Stall	A>1 Post Stall
Potential Lift C_{LP}	N/A (Stalled)	Equation 12	N/A (Stalled)
Vortex Lift C_{NV}	Equation 7	Equation 8	TBD
Pressure Drag C_{NN}	Equation 9	Equation 10	Equation 11

The slopes of linear aerodynamic force coefficients representing Equations 7, 8 and 12 are shown in Fig. 10 with the applicable regions identified. Here, the Prandtl-Betz experimental data are left as a reference, although those data reflect only the potential lift coefficient slopes whereas the theoretical values here are for normal forces and the truncated potential lift. A few normal force coefficient data points deduced from the Lamar test results [7] are also added as a reference, indicating an excellent agreement with the present theory. It is seen that, for A>1, the sum of normal force (Eq. 8) and the truncated potential lift (Eq. 12), provides the total force, consistent with the experimental data trends

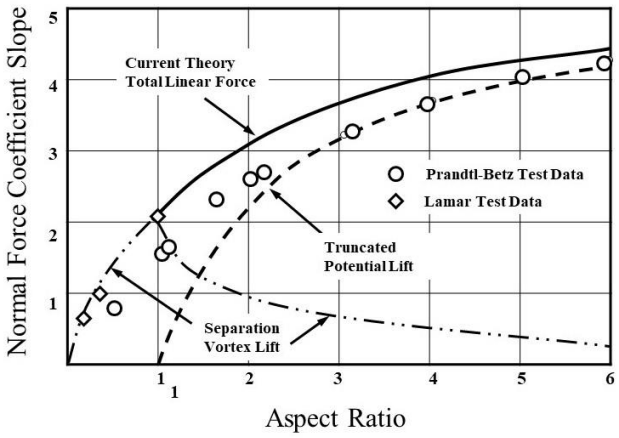

Figure 10 Current Theory Normal Force Coefficient Slope

3. VERIFICATION OF RESULTS

In Fig. 11, the theoretical results are compared to experimental data for narrow plates (A<1) by Lamar. It is seen that except for very high angles of attack in low aspect ratio cases, the data fit perfectly with experiments in all cases. The matching of the lift curves in the lower angle of attack range amply demonstrates that the separation vortex force is indeed a linear function of sin α. On the other hand, the agreement in drag values shows that the forces are truly normal to the wing surface and that the non-linear pressure drag applied here provides the proper magnitude augmenting the vortex force.

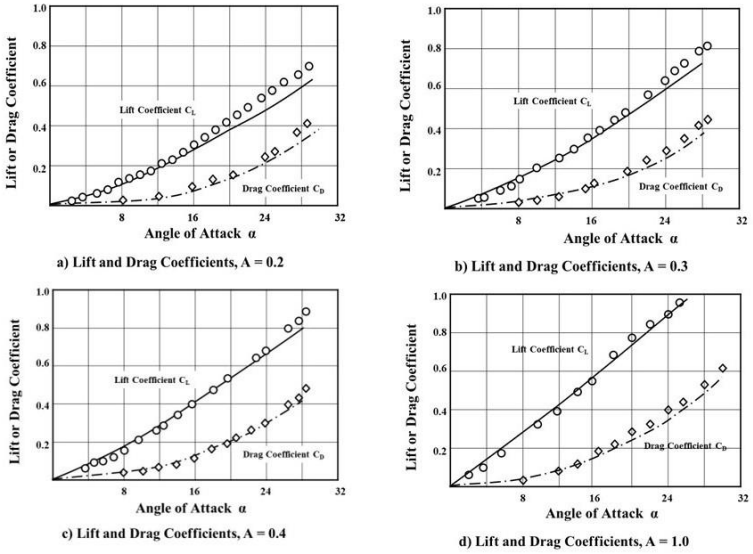

Figure 11 Verification of Lamar Data, A<1

The upswing of lift and drag at higher angles of attack, in very slender cases, is somewhat surprising. This could perhaps be conjectured as the result of a leading-edge separation bubble that appears at a high angle of attack, as suggested by Katz [10], or some other secondary effects. This is, of course, beyond the scope of the current investigation.

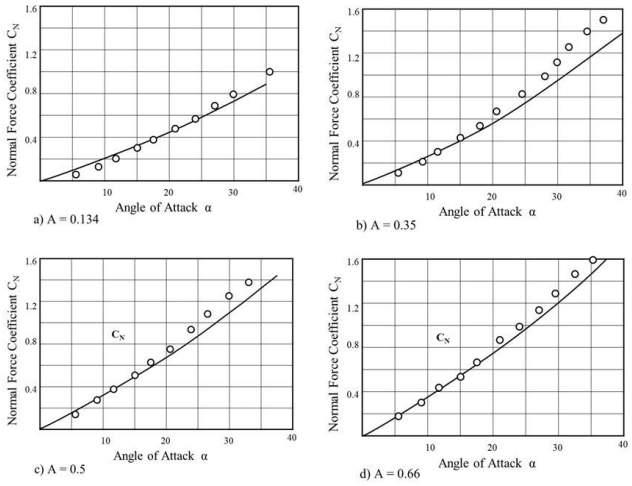

Figure 12 Verification of Winter Data, A< 1

The theory is also verified against the classical Winter data [12] as transcribed from Katz [10], in Fig. 12 and 13, for slender wings. The accuracy of the results is, again, equally remarkable.

Most noticeable in the square plate case (Fig. 13) is that the normal force is curving slightly upward before stalling at a very high angle of attack. Since the sine function should be a curve concaving slightly downward whereas the sine square term tends to raise it up, only a properly adjusted linear and non-linear force combination would give such a result. This is indeed the case presented here. The two effective force components are also shown in the diagram to highlight

their contributions. Notice that, here the result is obtained from the application of Eq. 8 and Eq. 10, one a theoretical deduction and the other a direct adoption of experimental data. The perfect match leaves little doubt about the validity of the current theory.

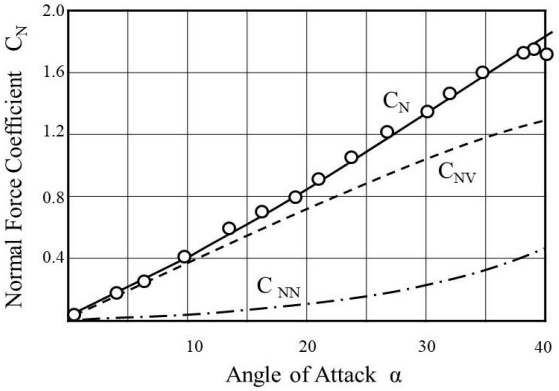

Figure 13 Verification of Winter Data, A= 1.0

The higher aspect ratio cases are evaluated against the Winter test data as well, Fig. 14. Here, the test data is adjusted for the zero angle of attack lift values. Again, the theory and experiments exhibit excellent agreements. In these cases, the "truncated potential lift" (Eq. 12), is deployed while the vortex lift and pressure drag contributions are reduced according to the area ratio of flow separation. This direct apportioning of lift data according to the vortex separation affected areas is demonstrated to be effective and accurate.

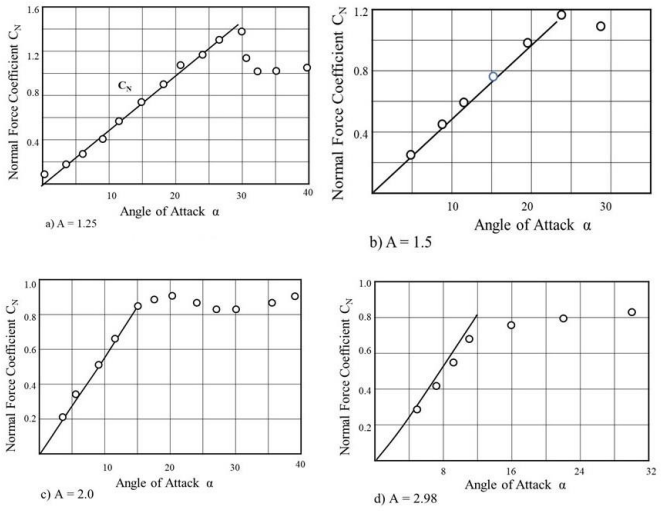

Figure 14 Verification of Winter Data, A> 1

It is interesting also to observe that stalling of these wider planforms occurs progressively earlier than narrow wings, and the behaviour is also much different. Take, for example, the case of A=2.0, Fig. 14 c), the initial stalling occurs around 15 degrees, however the total force coefficient stays high with some early reduction but then increases gradually again at a much slower rate without an abrupt reduction. It appears that the potential lift may be undertaking a gradual reduction before disappearing altogether. This behaviour is reminiscent of the "vortex bursting"

phenomenon in delta wings, a progressive disruption of the separation vortices starting from the trailing edge affecting the lift forces. These cases mandate a more thorough investigation of post stall behaviour now that a basic framework for pre-stalling lift is established.

One aspect so far not mentioned in the discussion is that, in view of the wing and flow geometry, the separation vortex normal force and the non-linear pressure drag are both exerted at or near the mid-chord of the plate. The vortex force, as shown, is applied to the wing centreline while the pressure drag spread almost uniformly to the end zones. This means that the two forces are both exerted at mid-chord. As Lamar noted, the experimental data demonstrates a "nose down" moment against the quarter chord location, the current theory supports this trend.

As discussed earlier that Hoerner, [5], indicated in the narrow wing range, the SWT solution falls short of test data, requiring a substantial non-linear "second lift" element to make up the differences. He estimated, from the bell-shaped lift coefficient slope-aspect ratio distribution, requiring a peak non-linear lift slope value of 3.6 at an aspect ratio around 0.7. The theoretical result from this study is checked against his interpretations in Fig. 15. Since Hoerner's demonstration is comparing against the SWT theory potential lift, the current evaluation needs to make proper adjustments to match the parameters. The sum of the first two terms in Eq. 13 is adjusted by subtracting the theoretical potential lift, in our case, Eq. 4, to obtain the equivalent excessive lift. This value is then divided by the sine of 16 degrees to emulate the appropriate "non-linear" lift coefficient slope and subsequently added to the non-linear pressure drag of Eq. 7 to reconstruct the Hoerner second lift.

As shown in Fig. 15, the adjusted theoretical result from this current research is in complete agreement with Hoerner's interpretation of the Winter data, proving that the second lift is only partially reliant on the non-linear lift (normal) force, while the linear vortex normal force makes a substantial contribution. The LESA non-linear suction lift parameter employed by Lamar [7] is also shown in the diagram demonstrating significantly different characteristics.

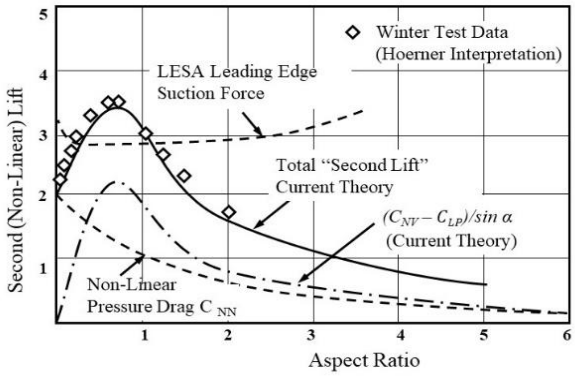

Figure 15 Verification of Hoener "Second Lift"

Finally, as a side note of interest, the crossflow vortex force expression (Eq. 7), does provide a "drag polar" relationship reminiscent to the classical LLT theory,

$$C_{DNV} = \frac{C^2{}_{LNV}\left[\frac{6(1+A^2)}{3+A^2}\right]}{2\pi A \cos^2\alpha} \cong C^2{}_{LNV}/\pi A \qquad (15)$$

The results agree in the low aspect ratio and small angle of attack limits. The wider wing cases can also be determined from the current theory by engaging the appropriate established equations.

4. CONCLUSIONS

The theory presented in this paper offers a comprehensive understanding of the aerodynamics of rectangular wings or flat plates. Included are an alternative geometry-based formulation for linear lifts, as well as a geometry-based empirical expression of pressure drag experimental data. The key contribution of this research is the identification and mathematical representation of the crossflow separation vortex mechanism, which plays a central role in lift production for slender wing cases. To the author's knowledge, this linear normal force has not been identified previously. Although not explicitly demonstrated, the theory has the potential to evaluate the aerodynamic moments applied to the wing. Moreover, the location of the normal forces could enable spanwise bending moment evaluations, as well as yawing and rolling behaviours, which could be explored in future research.

The common notion of "induced drag" forces is shown, in fact, to be the projections of the linear and non-linear normal forces, resulting in very similar outcomes to the "drag polar relationship" of classical theory.

One may argue that the vortex impulse approach really is not much different from the classical lift analysis. Indeed, after substituting the derivatives in Eq. (7), the expression in the integral is nearly identical to the potential lift in Eq. (5). The difference is that the current method could provide the explicit identification, interpretation, and evaluation of the crossflow separation vortex contributions, unbeknown previously.

Milne-Thomson himself employed this method to obtain the lift and drag relationship for the Prandtl finite wing problem. However, since he adopted the same elliptic lift distribution and utilized the induced downwash concept, he found no additional insights, and the vortex impulse theory has been neglected ever since. In fact, the theory may be viewed as a generalized Trefftz Plane Analysis approach that could and should be promoted in the future as a common methodology for both potential and vortex lifts for all planform geometries.

Although the equations developed in this study are approximate and empirical in nature, they are grounded in the mechanics of fluid motions and yielded explicit algebraic equations that can be easily scrutinized. The results have primarily been validated using experiments with flat plates of low to medium aspect ratios, but they are expected to be applicable to profiled wings and broader configurations as well. The highly accurate algebraic equations can serve as the basis for modelling aircraft flight dynamics, assessing engineering designs, and establishing reference values for CFD simulations. Work is in progress to extend the theory and methodology to other planform geometries.

REFERENCES

[1] Prandtl, L., and A. Betz .. "Experimentelle Prfifung der Umrechnungsformeln. Ergebnisse der AVA," Gottingen, 1920

[2] Prandtl, L., "Tragfltigel theorie. I. Mitteilung", Nachrichten der Koniglichen Gesellschaft der Wissenschaften zu Gottingen, Math. Phys. Klasse, 1918

[3] Schlichting, H, E. Truckenbrodt and H. Ramm, "Aerodynamics of the Airplane", MacGrow-Hill, New York, 1979

[4] Rom, J., "High Angle of Attack Aerodynamics", Springer-Verlag, New York, USA, 1992

[5] Hoerner, S. F. and H. V. Borst., "Fluid-Dynamic Lift," 3rd ed., Hoerner, Midland Park, N.J., 1975, PP 18-5
[6] Polhamus, E. C., "Predictions of Vortex-Lift Characteristics by a Leading-Edge Suction Analogy," AIAA J. Aircraft, Vol 8, 1971
[7] Lamar, J. E., "Extension of the Leading-Edge-Suction Analogy to Wings with Separated Flow Around the Side Edges at Subsonic Speeds," NASA TR R428, Washington D.C., 1971
[8] Milne-Thomson, L. M., "Theoretical Aerodynamics," 4th Edition, Constable and Company, Ltd., London, G.B., 1973
[9] Lee, S., "The Vortex Impulse Theory of Wing Aerodynamics," AIAA Paper AIAA-2004-4733, Presented at the 12th AIAA Applied Aerodynamics Conference, Providence RI, 2004
[10] Katz, J. and A. Plotkin, "Low Speed Aerodynamics," Cambridge University Press, Cambridge, UK, 2001
[11] Hoerner, S. F. "Fluid-Dynamic Drag," 3rd ed., Hoerner, Midland Park, N.J., 1965, PP 7-18
[12] Winter, H., "Flow Phenomena on Plates and Airfoils of Short Span," NACA, TM 798, 1936

AUTHORS

Dr. Shiang Yu Lee graduated from National Taiwan University and received his MME and Ph. D. degrees in Mechanical and Aerospace Engineering from University of Delaware in 1968. After initially involved in teaching and research activities, he joined the Boeing Company in 1978. He was initially involved in Structural Fracture Mechanics applications but spent most of his career in Information Technology working on ISO data exchange standards. After retirement in 2006, he focused on his passion of aerodynamics studies and presented several papers on wing theory and analysis.